Volume 15
Number 11
21 March 2024
Pages 1037-1134

# Polymer Chemistry

rsc.li/polymers

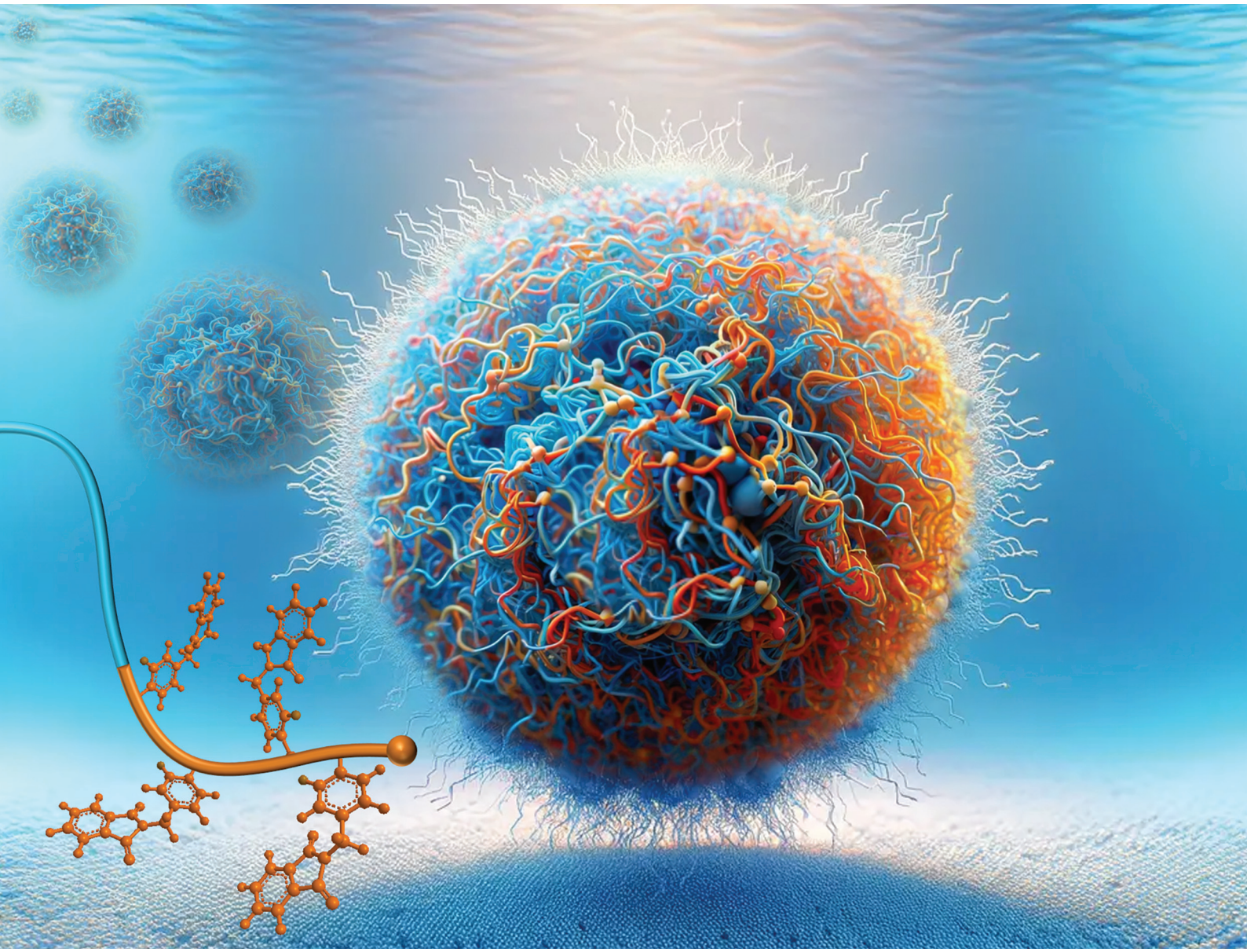

ISSN 1759-9962

ROYAL SOCIETY OF CHEMISTRY

**PAPER**

Shivshankar R. Mane and Andrea S. Carlini
Polymerization-induced self-assembly of (2-(4-vinylbenzyl) iso-indoline-1,3-dione) for the synthesis of hydrazine responsive block copolymer nanoparticles

Polymer Chemistry

ROYAL SOCIETY OF CHEMISTRY

PAPER

View Article Online
View Journal | View Issue



Cite this: *Polym. Chem.*, 2024, **15**, 1043

# Polymerization-induced self-assembly of (2-(4-vinylbenzyl)iso-indoline-1,3-dione) for the synthesis of hydrazine responsive block copolymer nanoparticles†

Shivshankar R. Mane *[a,b] and Andrea S. Carlini *[a,b,c]

Well-defined core–shell nanoparticles with a phthalimide core are synthesized using reversible addition–fragmentation chain transfer (RAFT)-mediated dispersion polymerization-induced self-assembly (PISA) of a novel vinyl benzyl phthalimide monomer, namely (2-(4-vinylbenzyl)iso-indoline-1,3-dione) (**VBzPHT**). Diblock copolymers consisting of poly(poly(ethylene glycol) methyl ether methacrylate)-*block*-(2-(4-vinylbenzyl)iso-indoline-1,3-dione) (**PEGMA$_{15}$-*b*-PVBzPHT$_n$**) self-assemble into nanoparticles during polymerization in methanol at 70 °C, when using poly(methyl ether methacrylate)-macro RAFT agent (macro-CTA, DP = 15, $M_n$ = 7600 g mol$^{-1}$, $Đ$ = 1.14) and 2,2′-azobis(isobutyronitrile) (AIBN) as an initiator. While maintaining a constant chain length of the solvophilic macro-CTA agent, we show that varying the solvophobic **PVBzPHT** block length (DP = 15–200) under concentrated conditions (15 wt%) achieves self-assembled structures of increasing size. These nanoparticles, ranging from 95 to 389 nm in hydrodynamic diameter, are assessed using both dynamic light scattering and dry state transmission electron microscopy. Finally, we investigate hydrazine-responsive deprotection of phthalimide bearing amphiphilic (**PEGMA$_{15}$-*b*-PVBzPHT$_n$**) block copolymers, leading to the formation of poly(poly(ethylene glycol) methyl ether methacrylate)-*block*-vinyl benzyl amine (**PEGMA$_{15}$-*b*-(PVBzNH$_2$)$_n$**). This increased solvophilicity leads to complex aggregated assemblies *in situ*. The insights of this study offer guidelines to the preparation of well-defined nanoparticles through PISA, with unique post-synthetic responsiveness amenable to applications in drug delivery and biocatalysis.

Received 20th January 2024,
Accepted 16th February 2024

DOI: 10.1039/d4py00073k

rsc.li/polymers



## Introduction

Mother Nature sets a perfect example of monodisperse polymers that achieve well-defined sizes and shapes.[1] This phenomenon inspires researchers to design amphiphilic homopolymers and block copolymers that self-assemble into nanoparticles such as micelles, vesicles, and worm-like structures *via* solution self-assembly. This can be done by interchanging single and mixed solvent systems or by slowly introducing new solvents to the solution under very dilute conditions (less than 1 wt% polymer).[2–12] In other instances, post-polymerization modifications to the polymer are used to modulate self-assembly, but this can be difficult to implement on a large scale.[13] Self-assembled nanoparticles have unique properties that are relevant to a wide range of applications, such as drug delivery, biocatalysis, bio-imaging, and protein immobilization.[14–18] Traditionally, higher-order morphologies[19,20] have been accessed by tuning the solvophobic–solvophilic balance (*i.e.* core and corona-forming blocks). However, precise control over size and shape of block copolymer assemblies at high solids content (10–50 wt%) in polar or non-polar solvents remains a key challenge.[21–23] In contrast, one-pot methods such as polymerization induced self-assembly (PISA) can access well-defined polymeric nanoparticles at high solid content, without the need for any post-polymerization modifications.[24,25]

In PISA block-copolymer formulations, a solvophilic precursor block is chain extended with another monomer to form a more solvophobic block. As this new block grows, the polymer chain becomes decreasingly soluble in the solvent system. Self-assembly of these polymer chains into nanoparticles then occurs when the growing block becomes insoluble at a critical degree of polymerization.[26–28] Reports of PISA in the last

[a]*Department of Chemistry and Biochemistry, University of California Santa Barbara, California 93106, USA. E-mail: srmane@ucsb.edu, acarlini@ucsb.edu*
[b]*Center for Polymers and Organic Solids, University of California Santa Barbara, California 93106, USA*
[c]*Department of Biomolecular Science and Engineering, University of California Santa Barbara, California 93106, USA*

†Electronic supplementary information (ESI) available: Monomer synthesis scheme and NMR data. See DOI: https://doi.org/10.1039/d4py00073k

decade primarily employ controlled/living polymerizations such as atom transfer radical polymerization (ATRP),[29–31] nitroxide-mediated polymerization (NMP),[32,33] ring-opening metathesis polymerization (ROMP),[34–37] living anionic polymerization (LAP),[38,39] ring-opening polymerization,[40,41] and reversible addition–fragmentation chain transfer polymerization (RAFT).[42–45]

The most common strategy, RAFT-mediated PISA, generally involves chain extension of a soluble macromolecular chain transfer agent (CTA) in a suitable solvent, followed by addition of a second soluble monomer. Despite the initial solubility of this second monomer, its respective insoluble polymer acts as the driving force for *in situ* PISA.[46–48] Most importantly, encoding these polymers with stimuli-responsive functional groups is gaining substantial interest in the context of PISA,[49,50] to further manipulate their shapes and sizes. This is achieved by shifting the amphiphilicity of diblock copolymer assemblies through molecular deprotection, rearrangement, crosslinking, or altering solvent conditions. External stimuli to initiate these transformations have been reported with light,[51,52] temperature,[53–55] and pH.[56] For example An and co-workers report temperature-sensitive poly(dimethylacrylamide)–poly(diacetone acrylamide) block copolymer nanoparticles, in which reversible morphological transitions from spheres to worms and lamellae are observed.[53] In another example, poly(*N*,*N*-dimethylacrylamide) shows a lower critical solution temperature that can be controlled by varying solids content and degree of polymerization.[54] Similarly, Zetterlund and co-workers employ RAFT dispersion PISA during the synthesis of P(*N*,*N*-diethylaminoethyl methacrylate)-*stat*-poly((ethylene glycol) methyl ether methacrylate) (PDEAEMA-*stat*-PEGMA), and observe that resulting particle morphologies can ranging from sphere to rods to vesicles through simple manipulation of pH and ionic strength.[56] Integral to accessing specific self-assembled and stimuli-responsive morphologies is the choice of initial core-forming monomer used during PISA.[57,58] Acrylates (MEA),[59] methacrylates (HEMA, DEGMA),[60,61] and acrylamides (NIPAM)[62] represent the most commonly employed monomers for dictating initial polymer morphologies. Despite extensive PISA efforts with a limited library of known core-forming monomers,[58] there remains a tremendous design scope for new monomers and those that bear stimuli-responsive functional groups.

Herein, we demonstrate for the first time a facile PISA synthesis of benzyl phthalimide-based block copolymer nanoparticles by using a newly identified hydrazine responsive core-forming monomer, vinyl benzyl phthalimide (**VBzPHT**) (Fig. 1). We use RAFT dispersion polymerization of **VBzPHT** with a block stabilizing poly((ethylene glycol) methyl ether methacrylate) (PEGMA) macro-chain transfer agent (macro-CTA). *In situ*, this produces poly(poly(ethylene glycol) methyl ether methacrylate)-*block*-(2-(4-vinylbenzyl)iso-indoline-1,3-dione) **PEGMA$_{15}$-*b*-PVBzPHT$_n$** diblock copolymer nanoparticles at high solids content (15 wt%) bearing hydrazine-responsive benzyl phthalimide group in their core. Tailoring the degree of polymerization prepares a series of **PEGMA$_{15}$-*b*-PVBzPHT$_n$** diblock copolymer nanoparticles with low dispersity. Hydrazine-induced deprotection of the resulting nanoparticles disrupts the balance of solvophobic core and solvophilic corona components, leading to particle disassembly and aggregation.

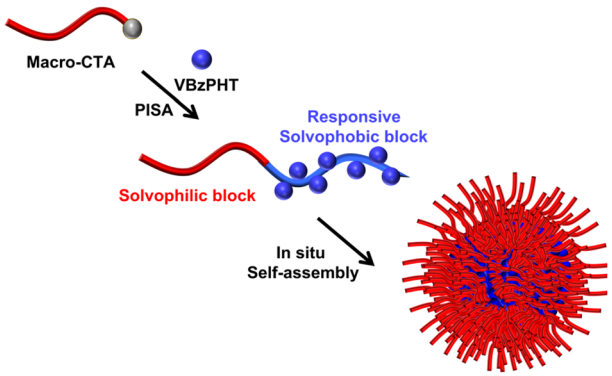


**Fig. 1** Synthesis of responsive block copolymer nanoparticles by reversible addition–fragmentation chain transfer (RAFT)-mediated polymerization-induced self-assembly (PISA).

## Experimental

### Materials

All the precursors as 4-vinyl benzyl chloride, potassium phthalimide and the RAFT-CTA agent 4-cyano-4-(phenylcarbonothioylthio)pentanoic acid were purchased from Sigma-Aldrich, and used as received. The 2,2′-azobis(isobutyronitrile) AIBN was also purchased from Sigma-Aldrich and recrystallized twice with methanol prior to use. The poly(ethylene glycol) methyl ether methacrylate (PEGMA) monomer ($M_n$ = 500 g mol$^{-1}$) was purchased from TCI and passed through alumina prior to use. All other reagents were used as received, unless otherwise noted.

### Monomer synthesis

In a round bottom flask, potassium phthalimide (15.77 g, 0.085 mol, 1.3 eq.) was dissolved in 100 mL DMF, to this 4-vinyl benzyl chloride (9.99 g, 0.0655 mol, 1 eq.) was added and the reaction mixture kept on heating at 110 °C for 6 h. After this reaction was cooled to room temperature, 400 ml water and 200 mL ethyl acetate were added to the solution. The aqueous layer was washed with ethyl acetate (3 × 100 mL) and dried over $MgSO_4$. The solvent was evaporated under reduced pressure and the obtained solid was re-dissolved in chloroform at 40 °C and precipitated in cold pentane. The crude product was filtered and washed with cold pentane. Finally, it was dried using high vacuum and to obtain **VBzPHT** as a free white powder (13.54 g, yield 80%).[63] $^1$H NMR in DMSO-d$_6$ ($\delta$ ppm): 7.75–7.95 (m, 4H), 7.45 (d, 2H), 7.25 (d, 2H), 6.72 (m, 1H), 5.77 (dd, 1H), 5.21 (dd, 1H), 4.79 (s, 2H). $^{13}$C NMR in DMSO-d$_6$ ($\delta$ ppm) 168.04, 137.17, 136.3, 135.91, 134.02, 132.07, 128.86, 122.45, 122.32, 114.15, 41.31.

### PEGMA-CTA (macro-CTA) synthesis

In a Schlenk tube, the desired amount of poly(ethylene glycol) methyl ether methacrylate (PEGMA) (2.863 g, 5.7269 mmol, 16 eq.) was taken and to this, RAFT-CTA 4-cyano-4-(phenylcarbonothioylthio)pentanoic acid (100 mg, 0.3579 mmol, 1 eq.) was added, followed by the addition of AIBN (5.877 mg, 0.03579 mmol, 0.1 eq.). All the solids were dissolved in 1,4-dioxane solvent at an inert atmosphere. The reaction mixture was degassed 3 times by freeze–pump–thaw cycle and kept in a preheated bath at 70 °C for 6 h. After complete polymerization, the reaction was quenched by sudden cooling of the tube in an ice water bath and exposure to air. The macro-CTA was obtained by several precipitation in cold dry diethyl ether. The molecular weight measured by SEC is ($M_n$ = 7600 g mol$^{-1}$, $Đ$ = 1.14). $^1$H NMR in DMSO-d$_6$ ($\delta$ ppm): 7.82 (dd, 2H), 7.64 (dd, 1H), 7.47 (d, 2H), 4.25–3.15 (m, PEG proton), 2.1–0.81 (m, background aliphatic protons).

DP and $M_{n,NMR}$ calculation: degree of polymerization for macro-CTA was calculated by $^1$H NMR spectroscopy (Fig. S3†).

$$\mathrm{DP}_m \text{ of PEGMA-CTA} = \frac{\frac{1}{3}\times \int_{3.15}^{3.29} (\text{--OCH}_3 \text{ proton}) \text{ signal ``i''}}{\frac{1}{5}\times \int_{7.41}^{7.93} (\text{Aromatic--CH proton}) \text{ signal ``a''}} = \frac{(45.22/3)}{(5/5)} = \sim 15$$

$$M_{n,NMR} = (\text{molecular weight of } \mathrm{PEGMA}_{500} \times \mathrm{DP}_m)$$

### RAFT dispersion polymerization for PEGMA$_{15}$-*b*-PVBzPHT$_n$ block copolymer synthesis

A typical RAFT dispersion polymerization for the synthesis of **PEGMA$_{15}$-*b*-PVBzPHT$_{50}$** block copolymer at 15 wt% total solid content was performed as follows: in a Schlenk tube equipped with a magnetic spin bar, 100.0 mg (0.0131 mmol) of macro-($M_n$ = 7600 g mol$^{-1}$, $Đ$ = 1.14), 173.21 mg (0.6578 mmol) **VBzPHT**, and 1.08 mg (0.0065 mmol) AIBN were taken. The entire solid was dissolved in 1.125 g of methanol at inert atmosphere. The reaction mixture was degassed 3 times by freeze–pump–thaw cycle and kept in a preheated bath temperature at 70 °C for 24 h. The polymerization reaction was stopped by sudden cooling the tube in an ice water bath, and exposing the solution to air. 100 μL of the resultant mixture was taken out for $^1$H NMR analysis to determine the monomer conversion, and a portion of the mixture was diluted with methanol followed by filtering through a 0.45 μm PTFE filter for TEM and DLS analysis. Finally, the **PEGMA$_{15}$-*b*-PVBzPHT$_{50}$** block copolymer was obtained by precipitation in cold dry diethyl ether and purified by several precipitations followed by vacuum drying at 40 °C for 12 h and measured SEC to obtain molecular weight ($M_n$ = 17 300 g mol$^{-1}$, $Đ$ = 1.08) see Table 1, P3. By targeting desired **PVBzPHT** block lengths, similar polymerization reactions were carried out by adjusting the feed ratio, which allowed access to spherical morphology.

DP and $M_{n,NMR}$ calculation: for the **PEGMA$_{15}$-*b*-PVBzPHT$_n$** (P1–P5) block copolymer, using $^1$H NMR spectroscopy (Fig. S6†).

$$\mathrm{DP}_n \text{ of PVBzPHT block} = \left(\frac{\frac{1}{8}\times\left(\int_{6.01}^{7.93} (\text{Aromatic--CH proton}) \text{ signal (``a + j + l'')} - \int_{7.41}^{7.93} (\text{Aromatic--CH proton}) \text{ signal ``a''}\right)}{\frac{1}{3}\times \int_{3.15}^{3.29} (\text{--OCH}_3) \text{ signal ``i''}}\right) \times \mathrm{DP}_m \text{ of PEGMA-CTA} = \frac{((405.40-5)/8)}{(44.74/3)} \times 15 = \sim 50$$

$$M_{n,NMR} = (\text{molecular weight of PEGMA-CTA}) + (\text{molecular weight of VBzPHT} \times \mathrm{DP}_n).$$

### Stimuli-responsive study control experiment

In a two-neck round bottom flask, 10.5 g of **VBzPHT** monomer was dissolved in 60 mL ethanol solvent and kept for heating at 40 °C followed by drop-wise addition of hydrazine monohydrate (7.68 mL). Finally, the reaction mixture stirred for 1 h at 40 °C and RT for 19 h. After the complete reaction, 100 mL of 10% KOH in water was added to maintain a pH 10 solution. The product was extracted from 3 × 100 mL chloroform and the organic layer was dried over $MgSO_4$ and solvent evaporated to yield **VBzNH$_2$**. $^1$H NMR in DMSO-d$_6$ ($\delta$ ppm): 7.23 (d, 2H), 7.15 (d, 2H), 6.51 (m, 1H), 5.58 (dd, 1H), 5.08 (dd, 1H), 3.61 (s, 2H). A similar protocol was employed for the **PEGMA$_{15}$-*b*-PVBzPHT$_n$** block copolymers P2 and P3 in water at ∼5 mg mL$^{-1}$. At 24 h incubation time, samples were collected and diluted with water to ∼1 mg mL$^{-1}$ for direct analysis by TEM and DLS. Samples for NMR analyses were precipitated and resuspended in DMSO-d$_6$ solvent.

### Polymer characterization

**NMR spectroscopy.** All the NMR spectra were recorded on a Bruker 500 MHz spectrophotometer or Bruker Avance-400 spectrometer using either DMSO-d$_6$ or $CDCl_3$ as a solvent. Typically, the samples were dissolved in deuterated solvent with an average of sixteen scans per spectrum. $^1$H NMR spectra of solutions in DMSO-d$_6$, and $CDCl_3$ were calibrated to tetramethyl silane as internal standard ($\delta$ 0.00).

**Size exclusion chromatography.** Molecular weight distributions were assessed by size exclusion chromatography (SEC) using DMF eluent. The DMF SEC system was equipped with two 5 mm (30 cm) Mixed C columns and a refractive index detector. The DMF mobile phase contained 2 v/v% triethylamine and 0.05 w/v% butylhydroxytoluene (BHT) and the flow rate was fixed at 1.0 mL min$^{-1}$. Poly(methyl methacrylate) used as an internal standard for calibration. A polymer sample of

5 mg was dissolved in 5 mL DMF and filtered with a 0.45 μm filter.

**Dynamic light scattering.** The particle size of the polymer was measured by dynamic light scattering (DLS) using a Zetasizer Nano-ZS instrument (Malvern Instruments) equipped with a 4.0 mW He–Ne laser operating at $\lambda$ = 633 nm at a scattering angle of 173°. All the samples were measured in aqueous as well as in methanol at room temperature. The average diameter and polydispersity (PDI) of the diblock copolymer particles were calculated. Data were averaged over thirteen run cycles each of thirty seconds time duration.

**Transmission electron microscopy.** Transmission electron microscopy (TEM) studies were conducted using FEI Tecnai T20 instrument. The TEM samples were prepared by dropping block copolymer solutions onto a carbon-coated 400-mesh copper grid.

## Results and discussion

### Monomer synthesis

Reacting vinyl benzyl chloride with potassium phthalimide at 110 °C (Scheme S1†) achieves synthesis of the core forming VBzPHT monomer. Confirmation by $^{1}$H and $^{13}$C NMR spectroscopy indicates appropriate monomer formation. The $^{1}$H NMR spectrum shows the appearance of characteristic signals at $\delta$ 7.75–7.95 ppm corresponding to the phthalimide proton, in addition to the vinylic backbone protons at $\delta$ 5.21–6.72 ppm (Fig. S1†). Similarly, in $^{13}$C NMR, the signal at $\delta$ 168.04 ppm denotes the phthalimide carbonyl group (amide), and $\delta$ 122.45, 132.07 ppm represent the aromatic carbons of the phthalimide ring (Fig. S2†).

### Synthesis of PEGMA$_{15}$-CTA (macro-CTA)

The RAFT solution polymerization of PEGMA in 1,4-dioxane solvent synthesizes macro-CTA at 70 °C by using 4-cyano-4-(phenylcarbonothioylthio)pentanoic acid as a RAFT agent, and

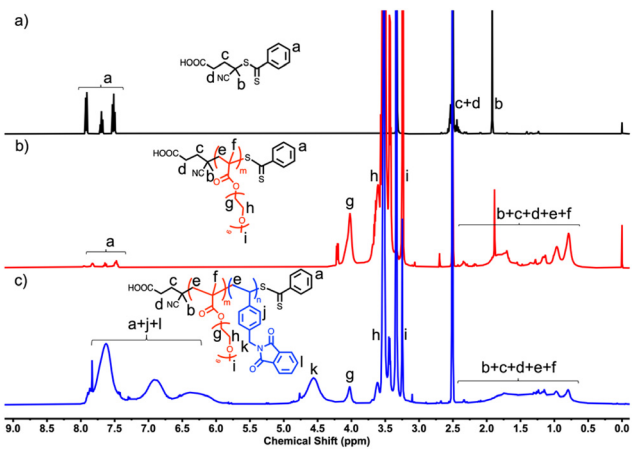


Fig. 2 $^{1}$H NMR overlay (a) RAFT agent, (b) macro-CTA, (c) **PEGMA$_m$-*b*-PVBzPHT$_n$** block copolymer in DMSO-d$_6$.

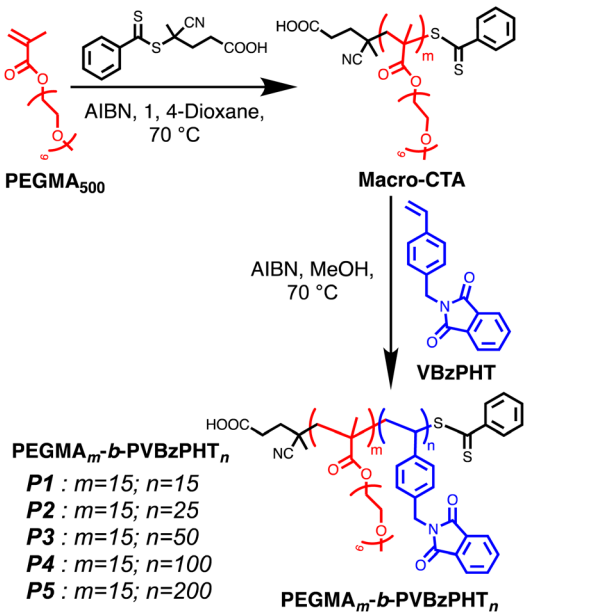


Scheme 1 RAFT-mediated synthesis of poly(poly(ethylene glycol) methyl methacrylate) (macro-CTA), followed by the synthesis of **PEGMA$_m$-*b*-PVBzPHT$_n$** block copolymer (P1–P5).

AIBN as a radical initiator. The polymerization reaction quenches after 6 h in ice cold water, leading to 94% monomer conversion. The molecular weight ($M_n$ = 7600 g mol$^{-1}$; $Đ$ = 1.14) of the macro-CTA was obtained from SEC, and the degree of polymerization (DP) of 15 was calculated from the monomer conversion (Fig. S3† and Table 1). A $^{1}$H NMR spectrum of **PEGMA$_{15}$** macro-CTA and its corresponding SEC curve are shown in Fig. 2b, S3,† and Fig. 3a respectively. The signals at $\delta$ 4.25–3.15 ppm correspond to PEG protons, in addition to this, the parent RAFT-CTA protons at $\delta$ 7.82–7.47 ppm along with methylene protons at $\delta$ 2.1–0.81 ppm confirm the formation of macro-CTA.

### RAFT dispersion polymerization for PEGMA$_{15}$-*b*-PVBzPHT$_n$ block copolymer nanoparticles

Poly(ethylene glycol) methyl ether methacrylate **PEGMA$_{15}$-CTA**, also known as macro-CTA, was used in the current study for RAFT dispersion polymerization of **VBzPHT** in methanol at 70 °C for 24 hours to *in situ* prepare nanoparticles of **PEGMA$_{15}$-*b*-PVBzPHT$_n$** block copolymer at 15 wt% total solids content (Scheme 1). Here we study how the size and shape of the nanoparticles evolve with the length of the solvophobic block, namely **PVBzPHT**, while keeping the chain length constant for macro-CTA. The target DP of the **PVBzPHT** chains sequentially increases from 15 to 200. The methanol solvent system is chosen for its ability to act as a good solvent for both the macro-CTA and **VBzPHT** monomer, but as a poor solvent for the **PVBzPHT** block, which is an essential basic condition for the PISA process to form *in situ* block copolymer nanoparticles. Thus, **PVBzPHT** block chains are insoluble in metha-

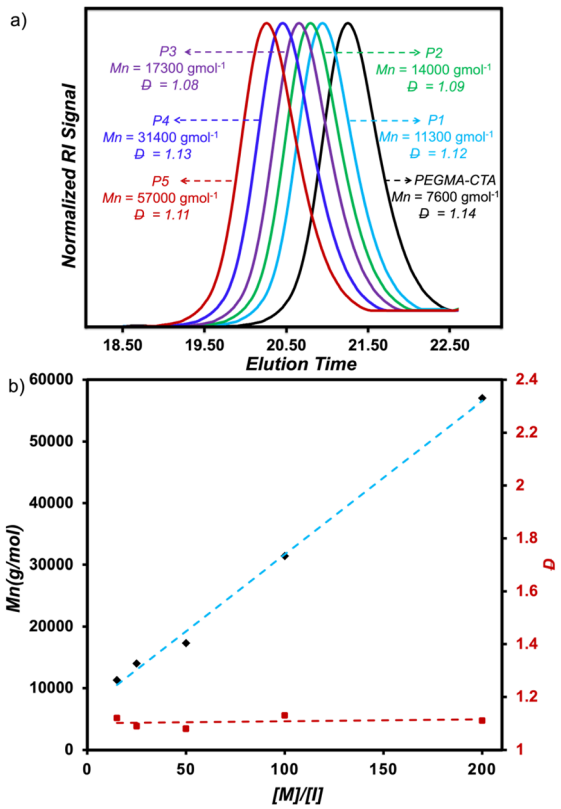


**Fig. 3** (a) Representative SEC traces for macro-CTA, and **PEGMA$_m$-*b*-PVBzPHT$_n$** block copolymer: P1–P5; (b) [M]/[I] *vs.* $M_n$ of P1–P5.

nol, which leads to the formation of *in situ* self-assembly by varying the DP of the core-forming **VBzPHT** monomer.

As the polymerization proceeds, the solution becomes turbid, indicating intra-strand nucleation as well as interstrand self-assembly of the **PEGMA$_{15}$-*b*-PVBzPHT$_n$** diblock copolymer. The polymerization reaction was analyzed by $H^1$ NMR spectroscopy and calculated the conversion (Fig. S4–S8†). The **VBzPHT** phthalimide aromatic protons corresponding to the broad signals from $\delta$ 7.93–6.01 ppm, the PEG protons at $\delta$ 4.25–3.15 ppm and the backbone methylene protons at $\delta$ 2.1–0.81 ppm confirms the diblock copolymer **PEGMA$_{15}$-*b*-PVBzPHT$_n$** formation. $^1$H NMR analysis indicates ~94% **VBzPHT** monomer conversion in each block copolymer case. Fig. 2 shows an overlay for the $^1$H NMR spectra of RAFT-agent, **PEGMA$_{15}$-CTA** and **PEGMA$_{15}$-*b*-PVBzPHT$_n$** diblock copolymer. 2D HSQC NMR of P1, P4, and P5 provide additional structural characterization (Fig. S9–S11†).

The molecular weight ($M_n$ = 7600 g mol$^{-1}$; $Đ$ = 1.14) of the macro-CTA followed by different block lengths (P1–P5; DP = 15–200) was measured by SEC. The observed molecular weight ranges from ($M_n$ = 11 300 g mol$^{-1}$ to 57 000 g mol$^{-1}$) with narrow dispersity ($Đ$ < 1.2). The normalized SEC traces for **PEGMA$_{15}$-*b*-PVBzPHT$_n$** along with macro-CTA were collected using a refractive index detector, as shown in Fig. 3 and Fig. S12.† The SEC curves shift towards a lower elution time as the degree of polymerization of the core-forming **PVBzPHT** block increases. This result suggests the complete initiation of macro-CTA, which results in the successful synthesis of a well-defined **PEGMA$_{15}$-*b*-PVBzPHT$_n$** diblock copolymer. Table 1 gives a summary of the results for **PEGMA$_{15}$-*b*-PVBzPHT$_n$** (P1–P5) diblock copolymer nanoparticles formed by RAFT dispersion polymerization in methanol.

Following the NMR and SEC analysis, all the **PEGMA$_{15}$-*b*-PVBzPHT$_n$** block copolymers were characterized using a combination of dynamic light scattering (DLS) and transmission electron microscopy (TEM) in methanol at 1 mg mL$^{-1}$. DLS experiments of **PEGMA$_{15}$-*b*-PVBzPHT$_n$** diblock copolymers show their nanoparticle assemblies possessing low dispersity values (0.16–0.32) and increasing hydrodynamic sizes with respect to increasing solvophobicity (Fig. 4 and Table 1). In the case of solvophilic P1, and P2 low dispersity particles with diameters of 95 and 118 nm, respectively. These sizes are maintained even after incubation in water for 24 h (Fig. S13†). As

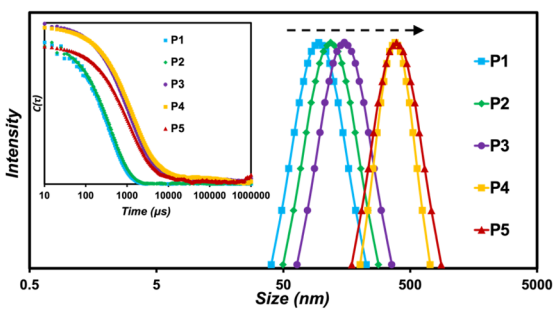


**Fig. 4** DLS analysis for **PEGMA$_m$-*b*-PVBzPHT$_n$** block copolymer (P1–P5) in methanol. Inset shows autocorrelation functions.

**Table 1** Summary of the results for **PEGMA$_m$-*b*-PVBzPHT$_n$** diblock copolymer

| Polymer | Composition | [M]/[I]$^a$ | Conversion$^a$ (%) | $M_n$$^a$ (g mol$^{-1}$) | $M_n$$^b$ (g mol$^{-1}$) | $Đ$$^c$ | Size$^d$ (nm) (PDI) |
|---|---|---|---|---|---|---|---|
| Macro-CTA | **PEGMA$_{15}$** | 15 | 94 | 7720 | 7600 | 1.14 | — |
| P1 | **PEGMA$_{15}$-*b*-PVBzPHT$_{15}$** | 15 | 93 | 11 545 | 11 300 | 1.12 | 95 (0.32) |
| P2 | **PEGMA$_{15}$-*b*-PVBzPHT$_{25}$** | 25 | 96 | 14 175 | 14 000 | 1.09 | 118 (0.32) |
| P3 | **PEGMA$_{15}$-*b*-PVBzPHT$_{50}$** | 50 | 94 | 20 750 | 17 300 | 1.08 | 151 (0.31) |
| P4 | **PEGMA$_{15}$-*b*-PVBzPHT$_{100}$** | 100 | 90 | 33 900 | 31 400 | 1.13 | 380 (0.16) |
| P5 | **PEGMA$_{15}$-*b*-PVBzPHT$_{200}$** | 200 | 94 | 60 200 | 57 000 | 1.11 | 389 (0.27) |

$^a$ Determined by $^1$H NMR spectroscopy. $^b$ Molecular weight (g mol$^{-1}$) determined by SEC in DMF. $^c$ Polydispersity index ($M_w/M_n$) determined by SEC. $^d$ Size and dispersity measured by DLS.

PISA progresses with longer solvophobic **PVBzPHT** blocks, nanoparticle sizes increase significantly, with diameters for P3–P5 being 151, 380 and 389 nm, respectively. Additionally, autocorrelation functions reveal a large shift in delay times between P2 and P3. This transition can be explained as a consequence of increasing the solvophobic block fraction that ultimately increases the packing parameter of diblock copolymer resulting from the formation of higher order morphologies.[64–66]

Amphiphilic polymers generated in this study show a high morphological dependence on solvation. Specifically, NPs with large solvophobic **VBzPHT** blocks (P3–P5) show increasing divergence between observed diameters by TEM and DLS. Unstained dry state TEM images show the morphology of our polymeric nanostructures (Fig. 5 and Fig. S14†). We observe discrete spherical nanoparticles of P1 and P2 by TEM, with observed diameters that closely agree with DLS data. However, TEM of polymers bearing larger solvophobic **VBzPHT** blocks (P3–P5) show increasing divergence between TEM and DLS results. This is exemplified by the observation of smaller, non-discrete, and lower contrast particles by TEM. We suspect that nanoparticle sizes of our more solvophobic polymers are more strongly influenced by drying effects during TEM sample preparation.[67] Specifically, polymeric core–shell nanoparticles bearing hydrated coronas, which contribute to hydrodynamic drag in DLS, are often collapsed in the desiccated and high-vacuum environment of TEM. To further investigate solvent effects, we precipitate our nanoparticles from methanol and resuspend them in water (pH ~ 6.0, for 24 h) as a control (Fig. S13†). Hydrophilic P1 and P2 display low sensitivity to these altered environmental conditions by DLS. In contrast, more hydrophobic P4 and P5 show a significant deswelling effect (>50%) from and 380/389 nm to 152/190 nm diameters, respectively as they exclude the more polar solvent. Therefore, unstained TEM morphologies are unlikely to be representative of solvated nanoparticles.

### Hydrazine-responsive study for $PEGMA_{15}$-*b*-$PVBzPHT_n$

The polymers presented in this manuscript were designed with a sufficiently high molecular weight corona-forming block to generate kinetically-trapped spheres. We suspect that reducing the hydrophobic core content *in situ* would enable the formation of higher-order morphologies. To do this, phthalimide protected amines can undergo deprotection by using hydrazine hydrate.[68,69] We demonstrate the responsive functionality of our **VBzPHT** monomer and resulting **$PEGMA_{15}$-*b*-$PVBzPHT_n$** block copolymers by subjecting them to hydrazine treatment for phthalimide deprotection. Upon addition of hydrazine hydrate, monomer deprotection of the phthalimide amine group occurs, therefore converting vinyl benzyl phthalimide (**VBzPHT**) to vinyl benzyl amine (**$VBzNH_2$**). Confirmation by $^1$H NMR spectroscopy after 20 h indicates the complete removal of phthalimide ring, as there is no signal at $\delta$ 7.75–7.95 ppm that corresponds to the phthalimide aromatic protons (Fig. S15†). Similarly, addition of hydrazine hydrate to particle solutions converts the solvophobic phthalimide block (**PVBzPHT**) of **$PEGMA_{15}$-*b*-$PVBzPHT_n$** polymer into solvophilic **$PEGMA_{15}$-*b*-$(PVBzNH_2)_n$**. For these experiments, we used P2 and P3 suspended in water, given their known stability in an aqueous environment (Fig. S13†). $^1$H NMR at 20 h shows a complete loss of signal for phthalimide at $\delta$ 7.25–7.95 ppm (Fig. S16 and S17†), indicating ~100% deprotection. The morphology of both deprotected nanoparticles by TEM (Fig. 6c and Fig. S19†) shows unique morphologies. For instance, treated P2 yields low contrast aggregated assemblies approximately 757 nm in size by DLS (Fig. S18a†). Conversely, treated P3 yields larger lamellae-like assemblies approximately 967 nm in size (Fig. S18b†). Fig. 6 depicts a schematic representation of the proposed disassembly and aggregation process for **$PEGMA_{15}$-*b*-$PVBzPHT_n$** to **$PEGMA_{15}$-*b*-$(PVBzNH_2)_n$**, with accompanying TEM images (Fig. S19†). We suspect that decreasing amphiphilicity, increasing solvation in water, and intermolecular hydrogen bonding between polymers

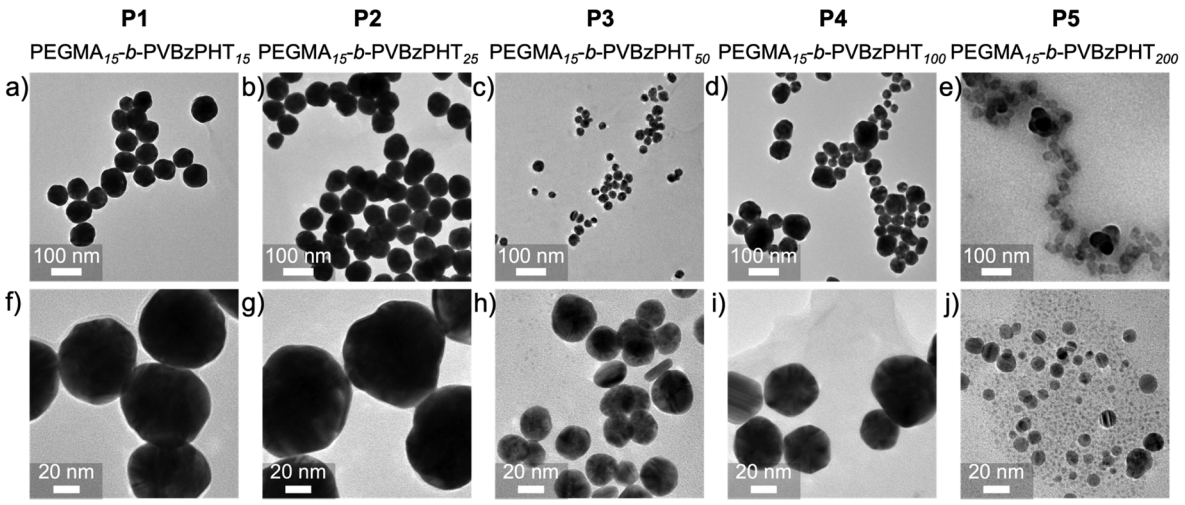


Fig. 5 Representative TEM images for **$PEGMA_{15}$-*b*-$PVBzPHT_n$** copolymer: P1 (a & f), P2 (b & g), P3 (c & h), P4 (d & i), and P5 (e & j).

 

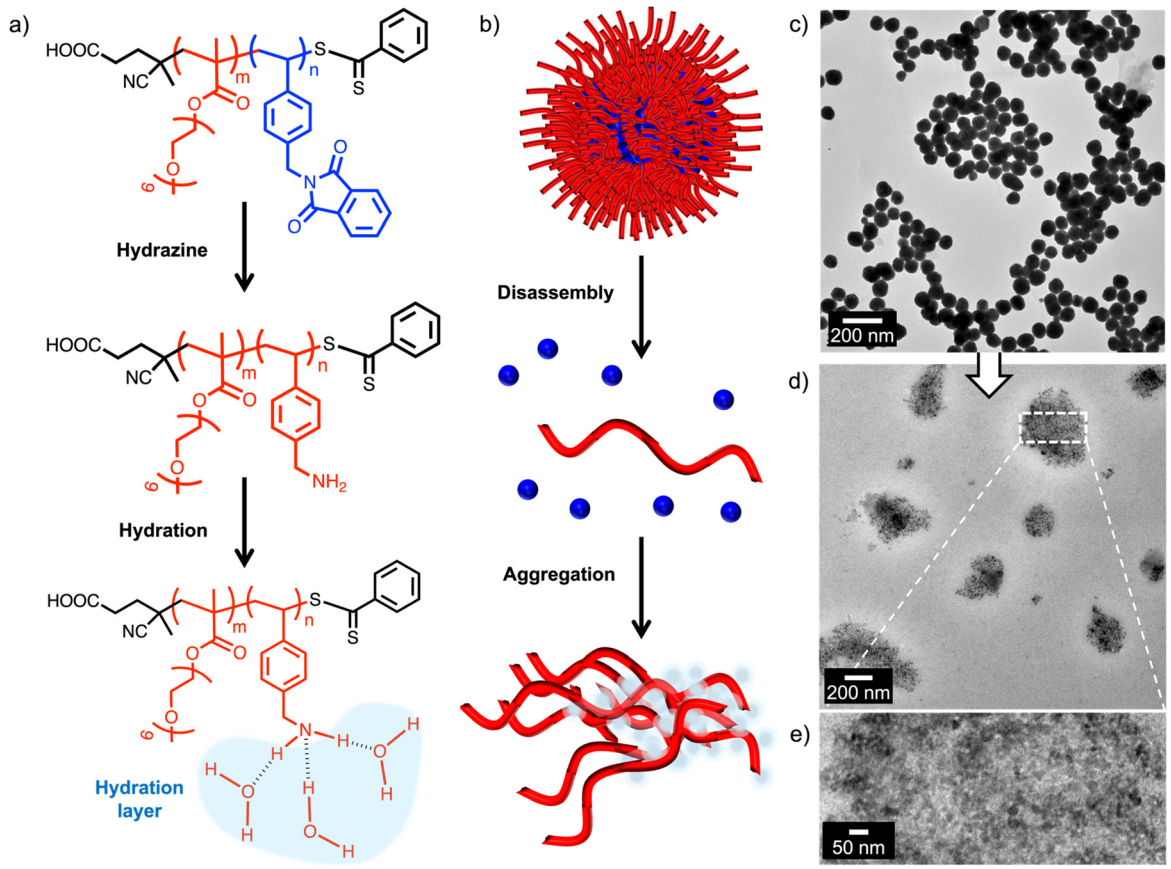


**Fig. 6** Schematic representation for disassembly of **PEGMA$_{15}$-*b*-VBzPHT$_n$** to **PEGMA$_{15}$-*b*-(VBzNH$_2$)$_n$**. (a) Chemical structure, (b) schematic disassembly and aggregation process, (c) representative TEM images for P2 before hydrazine treatment, (d & e) P2 after deprotection and aggregation after hydrazine treatment for 20 h.

with newly exposed amines are likely driving forces towards this molecular rearrangement.[70–72] The reduced crystallinity and increased sizes observed in treated P3 are likely attributable to the presence of twice the amount of hydrogen bonding and aromatic π–π stacking interactions between benzyl amines, in comparison to that of treated P2.

## Conclusions

In summary, the focus of this study explores RAFT-mediated dispersion polymerization-induced self-assembly of a newly identified benzyl phthalimide (**VBzPHT**) monomer. In combination with **PEGMA$_{15}$** macro-CTA, **VBzPHT** acting as the core-forming monomer for a variety of polymeric self-assembled nanoparticles. Variations in the chain length of the solvophobic block (DP 15–200), while maintaining a fixed length solvophilic macro-CTA, produces spherical morphologies ranging from 95 nm to 389 nm in diameter by DLS and TEM. Stimuli-responsive deprotection of the phthalimide bearing **PVBzPHT** core block results in structurally dynamic rearrangements into aggregated assemblies.

This PISA method represents a facile approach for the preparation of well-defined nanoparticles in which their unique responsive behavior poses a wide range of applications in drug delivery. Specifically, future studies aim to utilize the hydrazine-deprotected benzyl amine as a versatile linker for pH-responsive therapeutic cargos (*e.g.* doxorubicin conjugation *via* an imine linker).

## Author contributions

S. R. M. conceived the idea, and designed and performed the experiments. S. R. M. and A. S. C. analysed the data and wrote the paper.

## Conflicts of interest

The author declares no conflict of interest.

## Acknowledgements

S. R. M. would like to thank the CSIR-SRA (Scientist's Pool Scheme, Award No. 13(9139-A)/2020-Pool) for the funding. We thank the University of California and a UCSB Faculty

Research Grant for financial support. Thanks to Natasha Cao for manuscript revisions.

## Notes and references

1 J. Jennings, G. He, S. M. Howdle and P. B. Zetterlund, *Chem. Soc. Rev.*, 2016, **45**, 5055–5084.
2 D. E. Discher and A. Eisenberg, *Science*, 2002, **297**, 967–973.
3 Y. Mai and A. Eisenberg, *Chem. Soc. Rev.*, 2012, **41**, 5969.
4 R. J. Williams, A. P. Dove and R. K. O'Reilly, *Polym. Chem.*, 2015, **6**, 2998–3008.
5 B. M. Discher, Y. Y. Won, D. S. Ege, J. C. M. Lee, F. S. Bates, D. E. Discher and D. A. Hammer, *Science*, 1999, **284**, 1143–1146.
6 S. R. Mane, A. Sathyan and R. Shunmugam, *ACS Appl. Nano Mater.*, 2020, **3**, 2104–2117.
7 S. R. Mane, A. Sathyan and R. Shunmugam, *Sci. Rep.*, 2017, **7**, 44857.
8 G. Mellot, P. Beaunier, J. M. Guigner, L. Bouteiller, J. Rieger and F. Stoffelbach, *Macromol. Rapid Commun.*, 2019, **40**, 1–7.
9 S. R. Mane, K. Chatterjee, H. Dinda, J. Das Sarma and R. Shunmugam, *Polym. Chem.*, 2014, **5**, 2725–2735.
10 S. R. Mane and R. Shunmugam, *ACS Macro Lett.*, 2014, **3**, 44–50.
11 D. Kumar, S. A. Mohammad, A. Kumar, S. R. Mane and S. Banerjee, *Polym. Chem.*, 2022, **13**, 1960–1969.
12 T. I. Löbling, O. Ikkala, A. H. Gröschel and A. H. E. Müller, *ACS Macro Lett.*, 2016, **5**, 1044–1048.
13 K. Kita-Tokarczyk, J. Grumelard, T. Haefele and W. Meier, *Polymer*, 2005, **46**, 3540–3563.
14 D. Keller, A. Beloqui, M. Martínez-Martínez, M. Ferrer and G. Delaittre, *Biomacromolecules*, 2017, **18**, 2777–2788.
15 L. C. S. Huang, D. Le, I. L. Hsiao, S. Fritsch-Decker, C. Hald, S. C. Huang, J. K. Chen, J. R. Hwu, C. Weiss, M. H. Hsu and G. Delaittre, *Polym. Chem.*, 2021, **12**, 50–56.
16 S. R. Mane, I.-L. Hsiao, M. Takamiya, D. Le, U. Straehle, C. Barner-Kowollik, C. Weiss and G. Delaittre, *Small*, 2018, **14**, 1801571.
17 A. Beloqui, S. R. Mane, M. Langer, M. Glassner, D. M. Bauer, L. Fruk, C. Barner-Kowollik and G. Delaittre, *Angew. Chem., Int. Ed.*, 2020, **59**, 19951–19955.
18 Z. Wang, M. C. M. Van Oers, F. P. J. T. Rutjes and J. C. M. Van Hest, *Angew. Chem., Int. Ed.*, 2012, **51**, 10746–10750.
19 B. Charleux, G. Delaittre, J. Rieger and F. D'Agosto, *Macromolecules*, 2012, **45**, 6753–6765.
20 L. P. D. Ratcliffe, A. Blanazs, C. N. Williams, S. L. Brown and S. P. Armes, *Polym. Chem.*, 2014, **5**, 3643–3655.
21 M. Semsarilar, V. Ladmiral, A. Blanazs and S. P. Armes, *Langmuir*, 2013, **29**, 7416–7424.
22 Y. Li and S. P. Armes, *Angew. Chem., Int. Ed.*, 2010, **49**, 4042–4046.
23 X. Wang and Z. An, *Macromol. Rapid Commun.*, 2019, **40**, 1800325.
24 X. Zhang, S. Boissé, W. Zhang, P. Beaunier, F. D'Agosto, J. Rieger and B. Charleux, *Macromolecules*, 2011, **44**, 4149–4158.
25 S. Boissé, J. Rieger, K. Belal, A. Di-Cicco, P. Beaunier, M. H. Li and B. Charleux, *Chem. Commun.*, 2010, **46**, 1950–1952.
26 C. Liu, C. Y. Hong and C. Y. Pan, *Polym. Chem.*, 2020, **11**, 3673–3689.
27 N. J. W. Penfold, J. Yeow, C. Boyer and S. P. Armes, *ACS Macro Lett.*, 2019, **8**, 1029–1054.
28 S. L. Canning, G. N. Smith and S. P. Armes, *Macromolecules*, 2016, **49**, 1985–2001.
29 G. Wang, M. Schmitt, Z. Wang, B. Lee, X. Pan, L. Fu, J. Yan, S. Li, G. Xie, M. R. Bockstaller and K. Matyjaszewski, *Macromolecules*, 2016, **49**, 8605–8615.
30 Y. Wang, G. Han, W. Duan and W. Zhang, *Macromol. Rapid Commun.*, 2019, **40**, 1800140.
31 J. Wang, L. Yuan, Z. Wang, M. A. Rahman, Y. Huang, T. Zhu, R. Wang, J. Cheng, C. Wang, F. Chu and C. Tang, *Macromolecules*, 2016, **49**, 7709–7717.
32 X. G. Qiao, M. Lansalot, E. Bourgeat-Lami and B. Charleux, *Macromolecules*, 2013, **46**, 4285–4295.
33 X. G. Qiao, P. Y. Dugas, B. Charleux, M. Lansalot and E. Bourgeat-Lami, *Polym. Chem.*, 2017, **8**, 4014–4029.
34 D. B. Wright, M. A. Touve, L. Adamiak and N. C. Gianneschi, *ACS Macro Lett.*, 2017, **6**, 925–929.
35 J. C. Foster, S. Varlas, L. D. Blackman, L. A. Arkinstall and R. K. O'Reilly, *Angew. Chem., Int. Ed.*, 2018, **57**, 10672–10676.
36 D. B. Wright, M. A. Touve, M. P. Thompson and N. C. Gianneschi, *ACS Macro Lett.*, 2018, **7**, 401–405.
37 D. Le, M. Dilger, V. Pertici, S. Diabaté, D. Gigmes, C. Weiss and G. Delaittre, *Angew. Chem., Int. Ed.*, 2019, **58**, 4725–4731.
38 J. Wang, M. Cao, P. Zhou and G. Wang, *Macromolecules*, 2020, **53**, 3157–3165.
39 D. M. Day and L. R. Hutchings, *Eur. Polym. J.*, 2021, **156**, 110631.
40 E. Guégain, C. Zhu, E. Giovanardi and J. Nicolas, *Macromolecules*, 2019, **52**, 3612–3624.
41 J. Jiang, X. Zhang, Z. Fan and J. Du, *ACS Macro Lett.*, 2019, **8**, 1216–1221.
42 S. L. Canning, G. N. Smith and S. P. Armes, *Macromolecules*, 2016, **49**, 1985–2001.
43 M. Nardi, T. Scherer, L. Yang, C. Kübel, C. Barner-Kowollik and E. Blasco, *Polym. Chem.*, 2021, **12**, 1627–1634.
44 F. D'Agosto, J. Rieger and M. Lansalot, *Angew. Chem., Int. Ed.*, 2020, **59**, 8368–8392.
45 S. Piogé, T. N. Tran, T. G. McKenzie, S. Pascual, M. Ashokkumar, L. Fontaine and G. Qiao, *Macromolecules*, 2018, **51**, 8862–8869.
46 N. J. Warren and S. P. Armes, *J. Am. Chem. Soc.*, 2014, **136**, 10174–10185.
47 J. Cao, Y. Tan, Y. Chen, L. Zhang and J. Tan, *Macromol. Rapid Commun.*, 2021, **42**, 1–12.

 

48 S. J. Hunter, J. R. Lovett, O. O. Mykhaylyk, E. R. Jones and S. P. Armes, *Polym. Chem.*, 2021, **12**, 3629–3639.
49 F. D. Jochum and P. Theato, *Chem. Soc. Rev.*, 2013, **42**, 7468–7483.
50 F. D. Jochum, L. Z. Borg, P. J. Roth and P. Theato, *Macromolecules*, 2009, **42**, 7854–7862.
51 A. Bagheri, C. Boyer and M. Lim, *Macromol. Rapid Commun.*, 2019, **40**, 1800510.
52 C. A. Boyer and G. M. Miyake, *Macromol. Rapid Commun.*, 2017, **48**, 1700327.
53 X. Wang, J. Zhou, X. Lv, B. Zhang and Z. An, *Macromolecules*, 2017, **50**, 7222–7232.
54 C. A. Figg, A. Simula, K. A. Gebre, B. S. Tucker, D. M. Haddleton and B. S. Sumerlin, *Chem. Sci.*, 2015, **6**, 1230–1236.
55 S. Kessel, N. P. Truong, Z. Jia and M. J. Monteiro, *J. Polym. Sci., Part A: Polym. Chem.*, 2012, **50**, 4879–4887.
56 P. B. Zetterlund, D. Zhou, S. Perrier, R. P. Kuchel and S. Dong, *Polym. Chem.*, 2017, **8**, 3082–3089.
57 J. C. Foster, S. Varlas, B. Couturaud, J. R. Jones, R. Keogh, R. T. Mathers and R. K. O'Reilly, *Angew. Chem., Int. Ed.*, 2018, **57**, 15733–15737.
58 S. R. Mane, *New J. Chem.*, 2020, **44**, 6690–6698.
59 S. Sugihara, A. H. Ma'Radzi, S. Ida, S. Irie, T. Kikukawa and Y. Maeda, *Polymer*, 2015, **76**, 17–24.
60 K. Bauri, A. Narayanan, U. Haldar and P. De, *Polym. Chem.*, 2015, **6**, 6152–6162.
61 K. Parkatzidis, N. P. Truong, M. Rolland, V. Lutz-Bueno, E. H. Pilkington, R. Mezzenga and A. Anastasaki, *Angew. Chem., Int. Ed.*, 2022, **61**, e2021134.
62 X. Wang, C. A. Figg, X. Lv, Y. Yang, B. S. Sumerlin and Z. An, *ACS Macro Lett.*, 2017, **6**, 337–342.
63 S. Arias, E. Maron and H. G. Börner, *Biomacromolecules*, 2021, **22**, 213–221.
64 A. Blanazs, A. J. Ryan and S. P. Armes, *Macromolecules*, 2012, **45**, 5099–5107.
65 X. Dai, Y. Zhang, L. Yu, X. Li, L. Zhang and J. Tan, *ACS Macro Lett.*, 2019, **8**, 955–961.
66 Y. Mai and A. Eisenberg, *Chem. Soc. Rev.*, 2012, **41**, 5969–5985.
67 B. K. Wilson and R. K. Prudhomme, *J. Colloid Interface Sci.*, 2021, **604**, 208–220.
68 S. Srichan, H. Mutlu and J. Lutz, *Eur. Polym. J.*, 2015, **62**, 338–346.
69 J. W. Cleveland, J. Il Choi, R. S. Sekiya, J. Cho, H. J. Moon, S. S. Jang and C. W. Jones, *ACS Appl. Mater. Interfaces*, 2022, **14**, 11235–11247.
70 F. K. Wolf, A. M. Hofmann and H. Frey, *Macromolecules*, 2010, **43**, 3314–3324.
71 W. Qi, Y. Zhang, J. Wang, G. Tao, L. Wu, Z. Kochovski, H. Gao, G. Chen and M. Jiang, *J. Am. Chem. Soc.*, 2018, **140**, 8851–8857.
72 Y. Song, Y. Chen, P. Li and C.-M. Dong, *Biomacromolecules*, 2020, **21**, 5345–5357.